Quasi-static indentation modelling of aluminium specimen using finite element analysis

Mayank Nirbhay [a] , Mahima Dua [a] , Anurag Dixit [b] * , Satpal Sharma [a] , R. K. Misra [a]

[a] School of Engineering, Department of Mechanical Engineering, Gautam Buddha University, Greater Noida, 201312, India
[b] Department of Mechanical & Automation Engineering, G.B. Pant Government Engineering College, New Delhi, 110020, India

ARTICLE INFO

ABSTRACT

The influence of different types of rigid hemispherical and conical indenters on a rectangular specimen of aluminium has been investigated, in the small indenter test. A 3-D finite-element FE model was used to carry out the computation of the elastic-plastic solution of different rigid hemispherical and conical indenters. Three hemispherical-headed and four conical-headed indenters were designed and developed for testing. FE software ABAQUS® has been used to determine the load vs. indenter-displacement curves, reaction forces, deformation contours and Von-Mises stresses. The FE model was validated by comparing the results with the experimental data received from the Hertz Contact Theory and was found to be in reasonably good agreement.

1. Introduction

Using traditional and well-standardized mechanical test techniques, a component's adherence can hardly be evaluated, because enough material isn't sampled non-invasively from the components, so that the mechanical behaviour of materials can be determined. Thus, the small specimen test method has been utilized on a large scale, for calculating the damage of engineering components. In the small plate specimen method, a specimen in the form of a small disc is indented by a shaped penetrator at slow rate, deforming until failure is attained, and then the resulting load - displacement data is analysed. Manahan et. al. [1] modelled the small indenter test, by distortion of the disc, when a central load was applied and further determined the load vs displacement curve for a small plate specimen Manahan [2].

---

*Email : anuragdixitiitd@gmail.com

Originally, the small indenter test was taken as a miniature replacement for Charpy notch test. Baik et al. [3] made comparisons for the results of the Charpy notch test and the small indenter test, in determining the ductile brittle transition temperature (DBTT) of alloy steel at low temperature. Small square indenter specimens with dimensions of 10.0 mm x 10.0 mm x 0.5 mm were cut from previously tested Charpy specimens and were clamped around the periphery, and a central load was applied via a ball of 1.59 mm diameter. Load - displacement curves were obtained at low temperature.

Application for small indenter testing includes their use in nuclear generating systems and this test was also included in a number of small specimen techniques, which were used for irradiated samples by Lucas [4]. Mao et al. [5] also made studies on the small indenter test for irradiated materials. From this, it was concluded that the ductile-brittle transition temperature (DBTT) for small indenter testing of copper doped alloys was found to increase on neutron irradiation. Based on the load - displacement curves obtained from miniature specimen tests, Baik et. al. [3] and Cheon et. al. [6] described the deformation stages of a specimen during testing, which were classified into elastic bending, plastic bending, plastic membrane stretching, and plastic instability Okada et al. [7]. Platinum-based alloys for high temperature and special applications were used by Cornish et al. [8], while electric rock drilling system for in-stope mining in platinum operations was discussed in detail by Peitt [9].

Indentation testing [6] is a modern engineering technique, an alternative to other material parameter identifying methods, e.g. tensile testing. The purpose is to extract the loading and unloading force-displacement curves, from which useful data on the material's mechanical properties are obtained.

This investigation was aimed at examining the deformation behaviour of rigid hemispherical and conical headed indenters with different tip diameters, by performing experimental calculations based on the Hertz theory, as well as by finite-element simulations using ABAQUS® software. Finite element programs have become the most popular method for numerical analysis involving industrial and research applications. Many algorithms are used to solve the finite element set of equations, thus proper knowledge of these algorithms is necessary for models and their analysis. The ABAQUS® finite-element software with contact algorithm has been used for the determining the response induced, due to the quasi-static normal indentation of rigid indenters in the miniature sample [10].
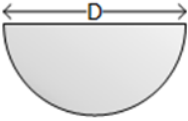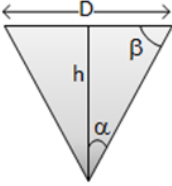
In the current work, hemispherical and conical indentation techniques Dixit et al. [11] have been used to evaluate the contact damage behaviour and damage tolerance properties of materials. A constant loading force was applied to the flat surface of the materials using conical and hemispherical indenters with different diameters in case of hemispherical indenters and different top angles in case of conical indenters. Validation further was done via Hertz contact theory and then the respective conical and hemispherical indenters, giving maximum and minimum value of Von-Mises stress and force have been visualised.

2. Finite Element Modelling

Finite element (FE) modelling is a cost-effective tool used to predict behaviour of composite materials under quasi-static indentation and low velocity. Some of the advantages of FE simulations are the flexibility to model either a localized region through the thick-

ness, or the entire structure and those geometric and material parameters can be easily varied. In the present work, 3D models of the test specimens and indenters were created in ABAQUS®. The diameter and thickness of cylindrical test specimens were 30 mm and 10 mm respectively. The indenters used for indentation were of hemispherical and conical geometries and their dimensions are shown in Table 1. The properties of aluminium, Young's modulus $(E) = 69$ GPa and Poisson ratio $(\nu) = 0.33$ were applied to test specimen. During modelling, the indenter was modelled as rigid body so that no deformation could occur to it and the specimen was modelled as deformable body. The assembly of the indenter and the miniature test was created, such that the indenter lies on the top of the test specimen at the centre, as shown in Figure 1. During analysis, surface to surface interaction was made between the indenter's outside surface and specimen's top surface. A tie constraint was also applied on the tip of indenter. The specimen was finely meshed using 8-noded 8640 C3D8R reduced integration elements. Three dimension 8-noded brick element with reduced integration (C3D8R) were found to be the most applicable element for these analyses, as brick elements have the ability to incorporate mid-side nodes (producing 21-node elements) and several material models. Eight-node element means, every element consists of 8 nodes, while reduced integration means that the order of integration is lower than that of full integration. The order of integration refers to single point in each element, which is placed at the centroid. Encastred boundary condition was applied to the bottom and cylindrical periphery of specimen. Also, the indenter was constrained to displace along the vertical axis only. In order to simulate the indentation process, the indenter was displaced vertically downward to 0.5 mm.

Table 1 – Geometry and dimensions of indenters used in simulation.

Indenter Geometry	Dimension				Figure
Hemispherical					

Type #	D (mm)
H1	10
H2	15
H3	20

Conical	D=20mm				

Type #	h(mm)	α	β
C1	17.3	30°	60°
C2	12.8	38°	52°
C3	10	45°	45°
C4	6	59°	31°

α = Half-cone tip angle
β = Top angle

3

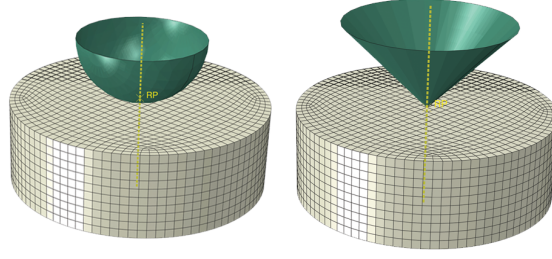**Fig.** 1 – Assembly of meshed specimen (ϕ=30mm and t=10mm) with hemispherical and conical rigid indenter.

3. Validation

Validation of the problem was performed using the Hertz Theory (Goodman et *al.* [12]). The theory of contact between elastic bodies has been used to find contact areas and indentation depths for simple geometries. The classical theory of contact or Hertz Theory focuses on non-adhesive contact or contacts, where no tension force occurs within the contact areas, thus the bodies in contact can be separated without adhesion forces. Complex forces and moments are transmitted between the bodies at their contact point. Also, the contact stresses have a nonlinear function of the deformation. So, to simplify the solution procedure, a frame of reference was considered in which the objects (in motion relative to each other) were static, and interacted through surface tractions (or pressures/stresses) at their interface.

According to Hertz Theory (Goodman et *al.* 1965), relation for calculating reaction force with respect to indentation depth is given by Equation 1.

$$F = \frac{2\sqrt{2}}{3} \frac{E\sqrt{D}}{1-\nu^2} d^{\frac{3}{2}} \tag{1}$$

The results of indentation were normalised using two parameters for indentation force and indentation depth, these two parameters have been expanded in Equation 2 and 3.

Dimensionless force,

$$D_F = \frac{F}{\pi R^2 E} \tag{2}$$

Dimensionless depth,

$$D_d = \frac{d}{R} \tag{3}$$

where

$F =$ Reaction force, $R =$ Radius of the hemispherical indenter, $d =$ Depth of indentation, $E =$ Young's Modulus of the specimen material, $\nu =$ Poisson's ratio of test material.

Initially, using Equation 1the value of theoretical force based on Hertz Theory was calculated and this value was applied in Equation 2 to obtain theoretical value of dimensionless force. Similarly, based on the value of reaction force obtained from simulation

contours shown in Figures 2 and 3(a), dimensionless force was calculated. All the calculated results are summarised in Table 2, showing that the analytical solution based on Hertz theory and FEM are approximately same.

Table 2 – Validation of FEM simulation results with Hertz theory results for hemispherical indenter of 10mm and 20mm diameter.

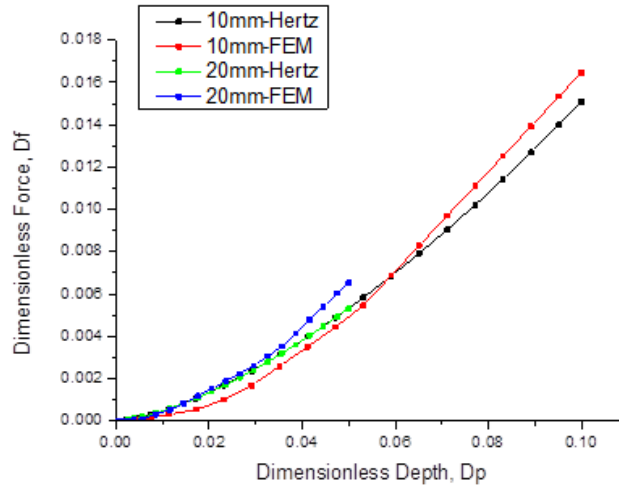| Diameter, D (mm)	Dimensionless Depth, D_d	Dimensionless Force, D_F	
	d/R	Hertz Theory	FEM
10	0.1	0.0150	0.0164
20	0.05	0.0053	0.0065

Fig. 2 – Dimensionless depth vs. dimensionless load for the hemispherical indenter.

4. Results and Discussion

In this section, results obtained from the indentation analysis of woven composites are discussed, individually for each indenter with the help of the distribution of Von Mises stresses and displacements plots. The stress plots provide information about the distribution of stresses around the point of indentation and also the induced displacement due to stresses. A parametric study was carried out with the aim to explore the effectiveness of the model, and to evaluate the influence of geometric and material parameters on the overall mechanical behaviour of the aluminium test specimen. Independent parameters, such as diameter of the hemispherical indenter and angles of the conical indenter, were varied and their effects on reaction force and material stiffness have been examined thoroughly.
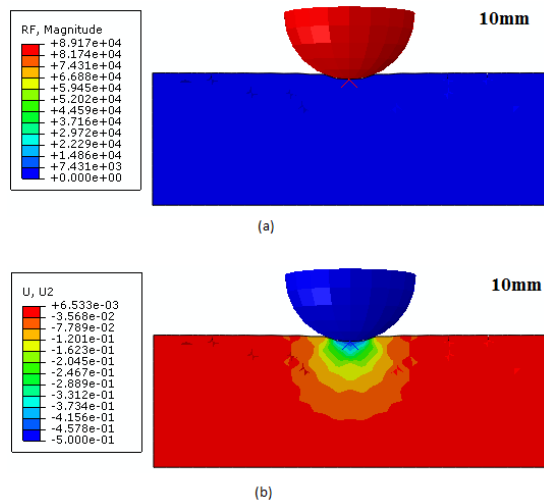
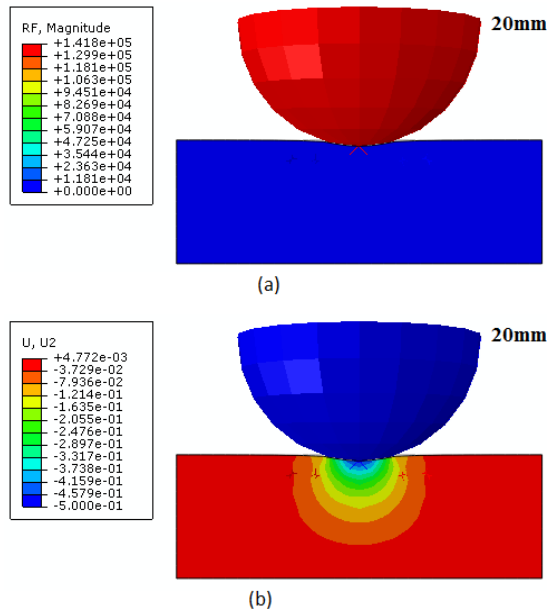**Fig.** 3 – (a) Reaction force; (b) Deformation contours in specimen with H1 type indenter.

Fig. 4 – (a) Reaction force; (b) Deformation contours in specimen with H3 type indenter.

Figure 4 shows the typical reaction force-indentation curves using hemispherical indenters of 10 mm, 15 mm and 20 mm, in which the reaction force was almost stable until the depth of indentation was 0.1 mm. On the other hand, beyond 0.1 mm indentation depth, gradual increase in reaction force was observed.

Furthermore, it was observed that indentation resistance depends on the size of the hemispherical indenter. From Table 3, the maximum load produced was for the diameter of 20 mm, and because with the increase in diameter, the area of the indenter in contact with specimen increased which results in gradually increased force.

Table 3 – Force (KN) corresponding to maximum displacement of the hemispherical indenter for different values of diameter.

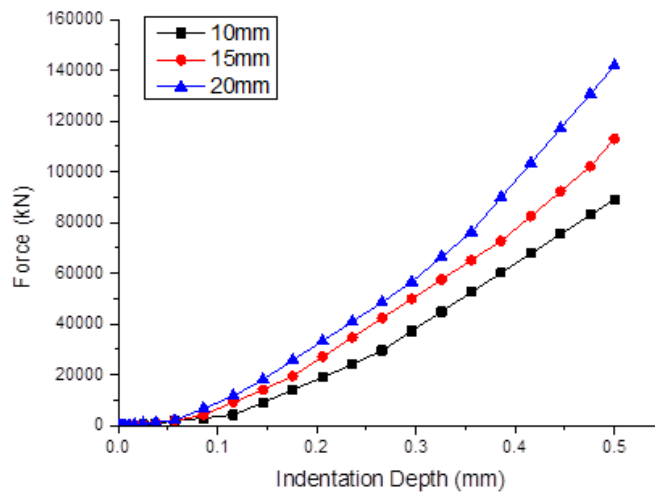| Diameter (mm)	10mm	15mm	20mm
Max. force (kN)	89174.8	112983	141762

Fig. 5 – Load vs. indentation depth graph for hemispherical indenters.

The behaviour of conical indenter was also investigated for four different types of indenters C1, C2, C3 and C4, Table 1. Figure 6 shows the reaction force-indentation curves with conical indenters. For each type of conical indenter, initially, a no crushing zone limit has been observed in specimen. The no crush zone limit corresponding to types C1, C2 and C3 indenters were 0.2 mm, 0.35 mm and 0.45 mm respectively, beyond this limit the indentation friction zone came into existence, and a gradual increase in reaction force was seen. For sharp cones (i.e. larger value of β, e.g. indenters C1 and C2), no crushing zone occurred in the specimen near the nose tip as shown in Figure 7. For blunt cones (i.e. smaller values of β, e.g. indenters C3 and C4), crushing zone were observed in the specimen near the nose tip, Figure 8. For conical indenters, the maximum and minimum loads were found for indenters type C4 and C1. The reason for this is for sharper indenters (i.e. minimum value of half cone angle α), penetration inside the specimen is easier and produces a low value of load as shown in Table 4.

Table 4 – Force (KN) corresponding to maximum displacement of the conical indenter for different values of top angles.

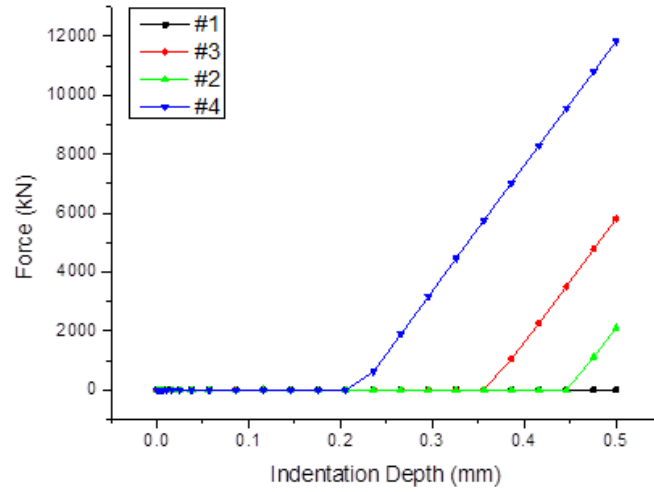| Half-cone angle (α)	30°	38°	45°	59°
Max. force (kN)	0	2110.98	5808.26	11826.9

7

Fig. 6 – Reaction force vs. indentation depth curves for type C1, C2, C3 and C4 conical indenter.
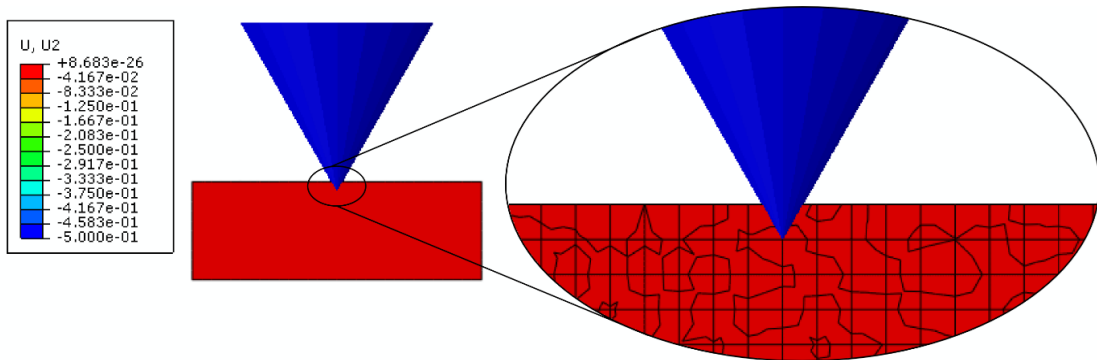

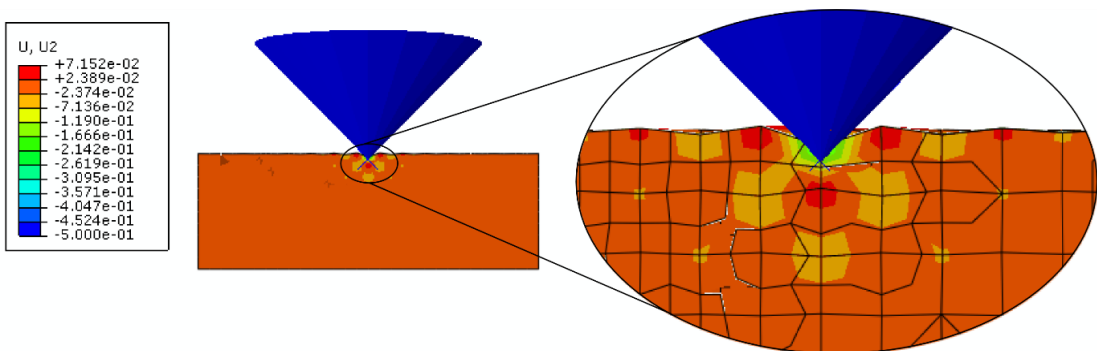**Fig.** 7 – No crushing zone in specimen near nose tip of type C1 indenter.

Fig. 8 – Crushing zone in specimen near nose tip of type C3 indenter.
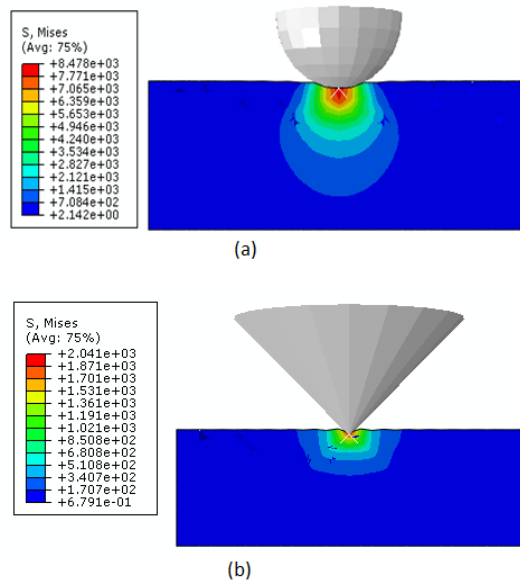
8

Fig. 9 – Section of specimen showing Von-Mises stress distribution due to indentation with (a) 10mm (H1) hemispherical indenter and (b) Type C3 conical indenter.
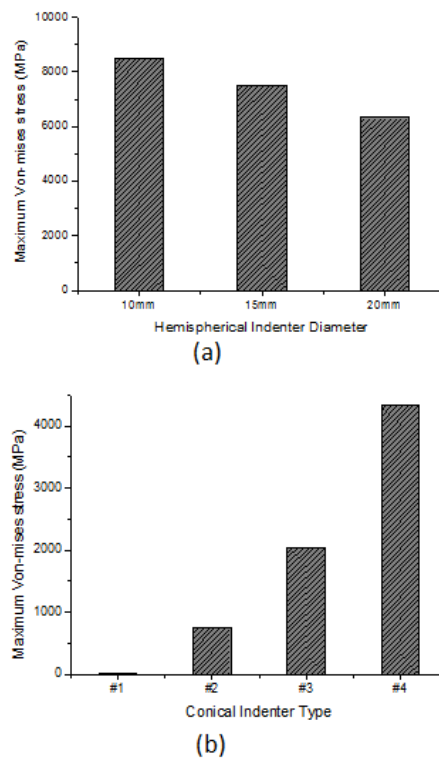

Fig. 10 – Maximum Von-Mises Stress (in MPa) for : (a) different diameters of hemispherical indenter and (b) for different types of conical indenter.

9

5. Observations

The stress distribution in case of hemispherical indenter was found to be through the thickness, whereas in case of conical indenter, the stresses were concentrated near the nose tip. Figure 9 shows the maximum Von-Mises stresses contours from contact damage produced on specimen during indentation with hemispherical and conical indenters. As the contact area with specimen increased in case of hemispherical indenter, the Von-Mises stress also decreased as shown in Figure 10 (a). Conversely, for conical indenter, the Von-Mises stresses increased as the half cone tip angle increased, as shown in Figure 10 (b).

6. Conclusions

(1) The deformation behaviour of the response induced in miniature samples, due to the quasi-static normal indentation of rigid hemispherical and conical headed indenters of different tip diameters and cone angles were modelled by performing the finite-element simulations. The model validated the computed load - displacement curves obtained by simulating all the three rigid hemispherical-headed indenters and four rigid conical-headed indenters on miniature test specimens with those obtained theoretically from the Hertz contact theory.

(2) The contact stresses between the test specimen and the rigid indenter were maximum at the edge of the contact area after yielding. However, the value of equivalent plastic strain was maximum at the centre of the bottom surface of the miniature test specimens. The stresses underneath the rigid indenter play a dominant role in the deformation.

(3) The effect of change in diameter of the rigid hemispherical headed indenters was discussed from contours of Von-Mises stresses, and the Von Mises stress decreased with increased indenter diameter. The Von-Mises stress was maximum for the H1 type indenter (8478 MPa), and minimum for the H3 type indenter (6326 MPa) at the ends of incremental steps.

(4) The effect of change in top angle of the rigid conical headed indenters was also derived from the contours of Von-Mises stresses, and these stresses increased with increased top angle. The Von-Mises stress was maximum for the C4 type indenter (43334 MPa) and minimum for the C1 type indenter (19 MPa) at the ends of incremental steps.

(5) The size of the damaged areas was found to be strongly dependent upon the indenter tip type. The largest and the smallest damage areas were found for the hemispherical and conical indenters respectively.

REFERENCES

[1] M.P. Manahan, A.S. Argon, and O.K. Harling, the development of miniaturised disk bend test for the determination of post-irradiation mechanical properties. J. Nuclear Mater, (1981) pp. 1545-550.

[2] M.P. Manahan, A new post-irradiation mechanical behaviour test. The miniature disk bend test. Nuclear Technology, vol. 63, (1983) pp. 275-295.

[3] I.M Baik, I. Kameda and O. Buck, Small indenter test evaluation of intergranu1ar embrittlement of an alloy steel. Scripta Metallurgica, vol. 17, (1983). pp. 1443-447.

[4] G.E. Lucas, Review of small specimen test technique for irradiation testing. Metallurgical Transaction-A, vol. 21A, (1990) pp. 1105-119.

[5] X. Mao, M. Saito and H. Takahashi, Small indenter test to predict ductile fracture toughness JIC and brittle fracture toughness KIC. Scripta Metallurgica, vol. 25, (1991) pp. 2481-485.

[6] S. Cheon, and S. Kim, Initial deformation during small indenter testing. J. Testing Eval., vol. 24, (1996) pp.255-62.

[7] A. Okada, M.L. Hanilton and EA. Garner, Microbulge testing applied to neutron irradiated materials. J. Nuclear Mater. (1991) pp. 179-181.

[8] L.A. Cornish, R. Suss, L.H. Chown, S. Taylor, L. Glaner, , A. Douglas, and S.N. Prins, Platinum-based alloys for high temperature and special applications. International Platinum Conference 'Platinum Adding Value', The South African Institute of Mining and Metallurgy. (2004) pp. 329-336.

[9] P.J. Petit, Electric rock drilling system for in-stope mining in platinum operations. International Platinum Conference 'Platinum Surges Ahead', The Southern African Institute of Mining and Metallurgy. (2006) pp. 209-216.

[10] A. Hussain, D.K. Sehgal and R.K. Pandey, Quasi-static Normal Indentation of a Circular Disk Shaped Miniature Specimen by Rigid Hemispherical-headed Punches. Defence Science Journal, Vol. 53, No.2, (2003) pp. 221-229.

[11] A. Dixit., R.K. Misra and H.S. Mali, Finite element analysis of quasi-static indentation of woven fabric textile composites using different nose shape indenters. Mat.-wiss. u. Werkstofftech., Vol. 46, No. 10, (2015) pp. 1014–1028.

[12] L.E. Goodman and L.M. Keer. The contact stress problem for an elastic sphere indenting an elastic cavity. Vol. 1, No. 4, (1965) pp. 407-415.